Low-temperature oxidation-induced crack healing in $Ti_2Al_{0.5}Sn_{0.5}C$–Al_2O_3 composites

Bei, Guoping; Mačković, Mirza; Spiecker, Erdmann; Greil, Peter

DOI
10.1111/ijac.13315

Publication date
2019

Document Version
Final published version

Published in
International Journal of Applied Ceramic Technology

Received: 27 May 2019 | Revised: 27 May 2019 | Accepted: 6 June 2019

DOI: 10.1111/ijac.13315

ORIGINAL ARTICLE

International Journal of Applied Ceramic TECHNOLOGY

Low-temperature oxidation-induced crack healing in $Ti_2Al_{0.5}Sn_{0.5}C$–Al_2O_3 composites

Guoping Bei[1,2] | **Mirza Mačković**[3] | **Erdmann Spiecker**[3] | **Peter Greil**[1]

[1]Department of Materials Science, Glass and Ceramics Group, University of Erlangen-Nürnberg, Erlangen, Germany

[2]Department of Materials Science and Engineering, Delft University of Technology, Delft, The Netherlands

[3]Department of Materials Science and Engineering, Institute of Micro- and Nanostructure Research (WW9) & Center for Nanoanalysis and Electron Microscopy (CENEM), FAU Erlangen-Nürnberg, Erlangen, Germany

Correspondence
Guoping Bei, Department of Materials Science and Engineering, Delft University of Technology, Mekelweg 2, 2628 CD Delft, The Netherlands.
Email: G.Bei@tudelft.nl

Funding information
German Research Foundation, Grant/Award Number: GR961/33-2; Cluster of Excellence, Grant/Award Number: EXC315

Abstract

The oxidation-induced crack healing of an Al_2O_3 composite loaded with various volume fractions of $Ti_2Al_{0.5}Sn_{0.5}C$ repair filler particles was investigated by annealing in air at a relatively low temperature of 700°C. After annealing a composite with 20 vol.% repair fillers (with a particle size of ~5.6 μm) for 48 hours, artificial indentation cracks prepared on the surface, as well as pores near the surface, were completely healed by filling with condensed oxidation products. Additionally, minor fraction of metallic Sn was detected. A complementary study by X-ray diffraction, transmission electron microscopy, scanning electron microscopy, and energy dispersive X-ray spectroscopy revealed that nano-sized oxidation products (SnO_2, TiO_2, and α-Al_2O_3 phase) were formed as major crack-filling species. After healing, the strength recovery of the Al_2O_3 composites was significantly improved in the composites loaded with more than 10 vol.% repair fillers and achieved 107% at 700 for 48 hours.

KEYWORDS

Al_2O_3-MAX phase composites, oxidation products, oxidation-induced crack healing, strength recovery

1 | INTRODUCTION

Engineering ceramics being able to repair cracks upon heat treatment have gained increasing attention.[1–3] Crack healing may offer a high potential for improving the reliability and prolongation of the lifetime of ceramic components subjected to mechanical loading at elevated temperatures.[1] Crack healing in ceramics via re-sintering (based on UO_2,[4,5] Al_2O_3,[6,7] ZnO,[8] MgO[9]), as well as oxidation of SiC, Si_3N_4, and related composites,[10–14] were reported as major crack-healing mechanisms giving rise for partial or even full recovery of the strength. The oxidation mechanism exhibits a more efficient healing ability than the re-sintering mechanism, because the volume expansion induced by crack surface oxidation can fill the crack gap more effectively. The enhancement of the crack-healing ability of those ceramics that are controlled by re-sintering mechanisms, was successfully achieved by loading repair fillers, such as SiC particles or whiskers in the ceramic matrix, featuring oxidation-induced healing.[15–22] Several parameters affecting the healing efficiency were investigated, such as healing temperature and time,[15] stress,[18] crack dimension,[19] and oxygen partial pressure,[20] as well as volume fraction and particle size of the repair filler constituent.[21] For example, an enhanced healing ability was observed in Al_2O_3 composites loaded with submicron-sized SiC particles as repair filler.[21] Decreasing the repair filler particle size from 270 to 30 nm resulted in lowering of the healing temperature from 1300 to 950°C, which was attributed to the activation energy for oxidation, scaling with SiC repair filler particle size.[21] The presence of an activator, such as MoO (0.2 vol.%) in the SiC–Al_2O_3 composite, was found to accelerate crack healing significantly, while strength recovery was achieved at 1000°C for 1 hour healing period.[22]

Recently, a group of ternary nitrides and carbides (MAX phases) with the general formula $M_{n+1}AX_n$ (n = 1 to 3), where M is a transition metal, A is an A group element, and X is either carbon or nitrogen,[23] demonstrated interesting healing abilities. MAX phases containing Al, such as Ti_3AlC_2,[24] Ti_2AlC,[25–27] and Cr_2AlC,[28] were reported to form a dense layer of α-Al_2O_3 filling in the gap. Compared with SiC- and Si_3N_4-based composites, larger cracks with a length of up to 7 mm and a crack opening width of up to 5 μm could be fully healed in Ti_3AlC_2 after heat treatment at 1100°C for 2 hours in air. Even a repeatable crack healing was observed in Ti_2AlC, indicating that MAX phases offer a multiple crack-healing ability. Furthermore, a Sn-containing MAX phase (Ti_2SnC) was able to repair millimeter-sized cracks by annealing at a relatively low temperature of 800°C within only 1 hour in air,[29] as well as in vacuum.[30] After healing, the flexural strength[29] and electrical conductivity[29,30] of the damaged material were almost fully recovered and reached the level of the virgin material. $Ti_2Al_xSn_{(1-x)}C$ MAX phase solid solutions were able to undergo oxidation-induced crack healing in ceramic composites at temperatures even below 1000°C.[29–33] The fracture strength of Al_2O_3 composites loaded with 20 vol.% of the $Ti_2Al_{0.5}Sn_{0.5}C$ repair filler containing artificial indent cracks, recovered fully to the level of the virgin material upon isothermal annealing in air atmosphere for 0.5 hours at 900°C.[32] However, the intrinsic healing mechanisms of $Ti_2Al_xSn_{(1-x)}C$–Al_2O_3 at temperatures even lower than 700°C have not been discovered yet. Thus, the scope of the present work was to examine the crack-healing behavior of Al_2O_3 composites loaded with $Ti_2Al_{0.5}Sn_{0.5}C$ repair filler operating at 700°C. An improved distribution of the repair filler in the Al_2O_3 matrix composites were obtained by reducing the particle size of repair filler. The healing efficiency was correlated with the oxidation and microstructure analysis of the healed zone of $Ti_2Al_{0.5}Sn_{0.5}C$–Al_2O_3 composites.

2 | EXPERIMENTAL DETAILS

The $Ti_2Al_{0.5}Sn_{0.5}C$ solid solution was synthesized from a reactant powder mixture, consisting of Ti, Al, Sn, and TiC (2 μm, 99% purity) with a molar composition corresponding to Ti-0.5Sn-0.5Al-0.9TiC. The annealing was conducted for 1 hour in vacuum at 1400°C. The reaction product was milled for 12 hours (Attrition mill with a ball-to-materials ratio of 2:1), resulting in a mean particle size of 5.6 μm (Mastersizer 2000, Malvern Instruments, UK). The Al_2O_3 matrix (AKP-53; Sumitomo Chemical, Japan) loaded with $Ti_2Al_{0.5}Sn_{0.5}C$ composites with repair filler fractions of 5, 10 and 20 vol.% were sintered at 1350°C for 4 hours in Ar atmosphere (Heraeus Holding GmbH, Hanau, Germany) by applying a heating rate of 5°C/min. Further details of the manufacturing process are given in Ref[30,31].

The $Ti_2Al_{0.5}Sn_{0.5}C$–Al_2O_3 composite, dedicated for mechanical investigation, was polished to 1 μm surface finish using a diamond suspension and cut into bar specimens with dimensions of 2.5 × 2.0 × 28 mm^3. The density of the materials was measured according to the Archimedes method. Surface cracks were generated by means of Vickers indentation, applying a constant load of 100 N (HV10) for 10 seconds (Zwick, Ulm, Germany). Oxidation-induced crack healing was carried out in an oxidation furnace (Linn High Term GmbH, Eschenfelden, Germany) at 700°C for 48 and 96 hours. The weight change of $Ti_2Al_{0.5}Sn_{0.5}C$–Al_2O_3 composites caused by oxidation reaction was recorded at 700 and 900°C for 12 hours by a thermal balance, applying a heating rate of 5°C/min (STA 429; Netzsch, Selb, Germany).

The phase composition prior and after the heat treatment was analyzed by X-Ray diffraction (XRD, Kristalloflex; Siemens AG, Mannheim, Germany) operated with monochromated Cu-K_α radiation. The composite microstructure and the indent crack morphology were analyzed by scanning electron microscopy (SEM, Helios NanoLab 600i FIB Workstation; FEI, Eindhoven, the Netherlands). After the healing treatment, the reaction products filling the crack space were examined by field emission SEM (FE-SEM) coupled with a focus ion beam (FIB, Helios NanoLab 600i FIB Workstation, FEI) system and energy dispersive X-ray spectroscopy (EDXS; Oxford Instruments INCA, Oxford, UK). Thin-section specimens were prepared by FIB, which is equipped with a Ga^+-ion source and operated at 30 kV. A protective platinum layer (30 × 2 × 5 μm^3) was deposited on the surface area of the selected healed zone. The lamella was finally thinned to 50-100 nm with a very fine ion beam current. Transmission electron microscopy (TEM) was performed with a Philips CM30 TWIN/STEM and Philips CM300 UltraTWIN (both from FEI Company), both operated at 300 kV acceleration voltage. TEM images and electron diffraction patterns were recorded using a charged couple device (CCD) camera from TVIPS (Tietz Video and Processing Systems GmbH, Gauting, Germany) with an image size of 1024 × 1024 pixels (at the CM30 TEM) and 2048 × 2048 pixels (at the CM300 TEM), respectively. The processing of the TEM images and diffraction patterns was performed with the free available software ImageJ (Version 1.48r) and the commercially available software DigitalMicrograph™. The evaluation of the electron diffraction patterns was performed by simulating the experimental diffraction patterns with the software JEMS (java version 3.5505U2010) and using the inorganic crystal structure database (ICSD) files for Al_2O_3 (#10425), SnO_2 (#9163), and TiO_2 (#9161).

The Gibbs free energy of various oxidation products, such as Al_2O_3, SnO_2, and TiO_2, was calculated by thermodynamic calculations using the FactSage 7.1 software.[34] The thermodynamic data of oxidation products Al_2O_3, SnO_2, and TiO_2 were taken from the FToxide database and the

thermodynamic data of metallic Al and Sn and Ti were taken from the Bins database.[34]

Filling of the crack space with condensed oxidation products causes the strength of the indented samples to recover. The flexural strength of the virgin sample, σ_0, indented sample, σ_{indent}, as well as healed samples after thermal treatment, σ_{heal}, were measured by three-point bending (5565; Instron Deutschland GmbH, Pfungstadt, Germany) using ASTM Standard (C1161-18), by applying a lower support span of 20 mm and a crosshead speed of 0.5 mm/min.

3 | RESULTS AND DISCUSSION

3.1 | Composite microstructure

Figure 1 displays the XRD pattern of the sintered $Ti_2Al_{0.5}Sn_{0.5}C$–Al_2O_3 composites loaded with 20 vol.% repair fillers. Only α-Al_2O_3 and $Ti_2Al_{0.5}Sn_{0.5}C$ solid solution were detected as crystal phases, indicating that the $Ti_2Al_{0.5}Sn_{0.5}C$ repair filler did not suffer from thermal degradation during the high-temperature sintering process. Figure 2 shows back scattering SEM images of sintered $Ti_2Al_{0.5}Sn_{0.5}C$–Al_2O_3 composites containing 5, 10, and 20 vol.% repair fillers. The MAX phase repair filler particles were uniformly dispersed in the alumina matrix. In accordance with the increasing volume fraction of the repair filler, the mean repair filler inter-particle distance, λ_{MAX}, calculated according to Ref. [35], decreased from $\lambda_{MAX} \approx 2.3$ μm (5 vol.%) to ~1.3 μm (20 vol.%), respectively (see Table 1). The repair filler inter-particle distances are significantly smaller compared to the lengths of the artificial cracks emanating from the load indents ($c_{indent} = 280 \sim 330$ μm). Figure 3 shows a typical microstructure of a crack emanating from the tip of the Vickers indentation in the Al_2O_3

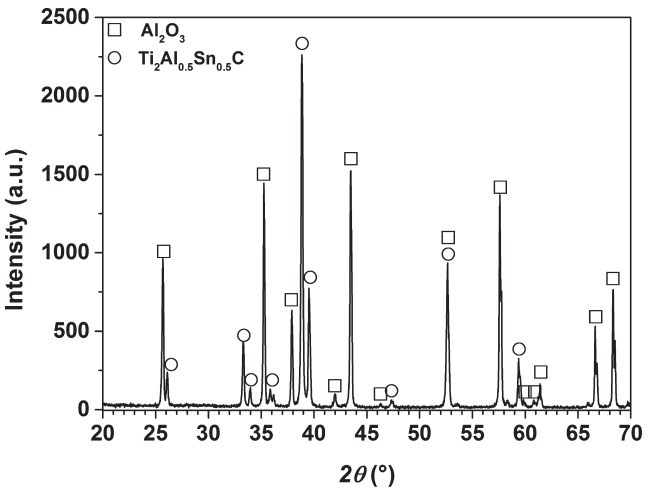

FIGURE 1 X-Ray diffraction pattern of the synthesized $Ti_2Al_{0.5}Sn_{0.5}C$–Al_2O_3 composites containing 20 vol.% repair fillers with a particle size of 5.6 μm

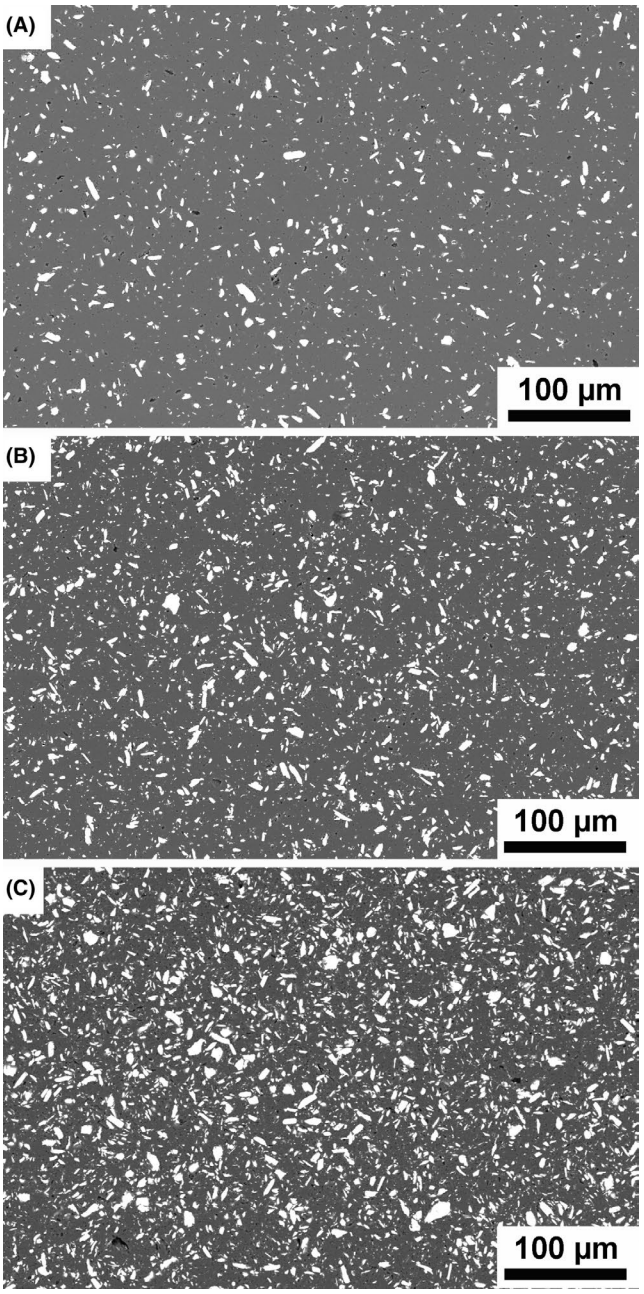

FIGURE 2 Scanning electron microscopy micrograph of Al_2O_3 composites sintered at 1350°C for 4 h in Ar atmosphere containing different volume fraction of $Ti_2Al_{0.5}Sn_{0.5}C$ MAX phase repair filler (A) 5 vol.%, (B) 10 vol.% (C) 20 vol.%

TABLE 1 Microstructure parameters of the prepared alumina composite specimens

Vol.%	5	10	20
Porosity (%)	2.1	2.8	7.6
d_{max} (μm)	4.8 ± 2.2	4.5 ± 1.4	4.5 ± 1.5
λ_{MAX} (μm)	2.3 ± 1.3	1.7 ± 1.2	1.3 ± 1.1
Indent crack length (μm)	345 ± 9	336 ± 4	328 ± 8
Indent crack width (μm)	0.43 ± 0.04	0.46 ± 0.05	0.32 ± 0.06

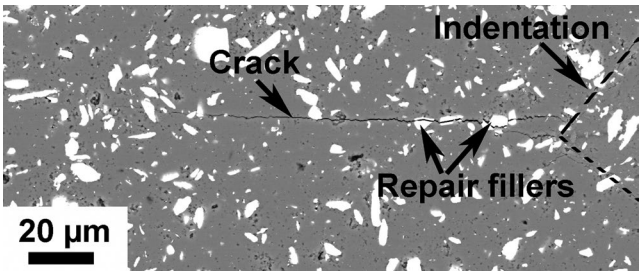

FIGURE 3 Vickers indentation induced crack formation in the Al_2O_3 composites containing 10 vol.% repair fillers with different particle size

composite containing 10 vol.% repair fillers. The repair filler particles are homogenously distributed around the crack path. A small prolongation of the crack length of 345 μm observed on composites with a minimum repair filler fraction of 5 vol.% may be attributed to a reduced toughness compared to an enhanced toughness at high particle loading fractions.

3.2 | Oxidation-induced crack healing

Annealing of the $Ti_2Al_{0.5}Sn_{0.5}C$–Al_2O_3 composites in air triggered a sequence of oxidation reactions of the $Ti_2Al_{0.5}Sn_{0.5}C$ repair filler, which resulted in the formation of Al_2O_3, SnO_2, and TiO_2 oxidation products (Figure 4). Although, the Gibbs free energy for Al_2O_3 formation is the lowest among the formed oxides (Figure 5), newly formed Al_2O_3 could not be detected by XRD due to overlapping Al_2O_3 matrix peaks. Metallic Sn was detected, which is likely to occur deeply in the crack where the local oxygen concentration is too low for tin oxide formation.[32]

Figure 6 shows the weight increase of the composite loaded with 20 vol.% $Ti_2Al_{0.5}Sn_{0.5}C$ during the thermogravimetric measurement at 700 and 900°C under same heating conditions. Oxidation reactions, indicated by a weight increase, started at about 450°C, which was in agreement with the oxidation behavior measured on the single phase $Ti_2Al_{0.5}Sn_{0.5}C$ powders.[36] While at 900°C a rapid reaction causes the weight gain to raise to 4.25 after 30 minutes, the oxidation reaction at 700°C proceeds much slower and reaches 3.3% after a holding period of 12 hours. Furthermore, time scaling changes from a linear relation at 900°C to a parabolic relation at 700°C. Figure 7 shows the microstructure of the healed crack after annealing at 700°C for an elongated period of 48 hours. Crack bridge formation and partial crack filling was observed on the composite loaded with 10 vol.% repair fillers, whereas complete crack filling occurred in the 20 vol.% specimen. EDXS mapping analysis confirmed the presence of TiO_2, SnO_2 and Al_2O_3 as major oxidation products, as well as a minor fraction of metallic Sn.

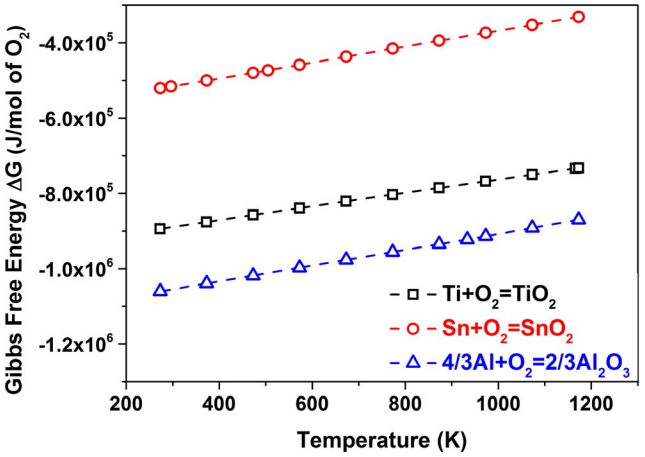

FIGURE 5 Standard Gibbs free energy of various oxidation reactions of M and A elements from the $Ti_2Al_{0.5}Sn_{0.5}C$ MAX phase

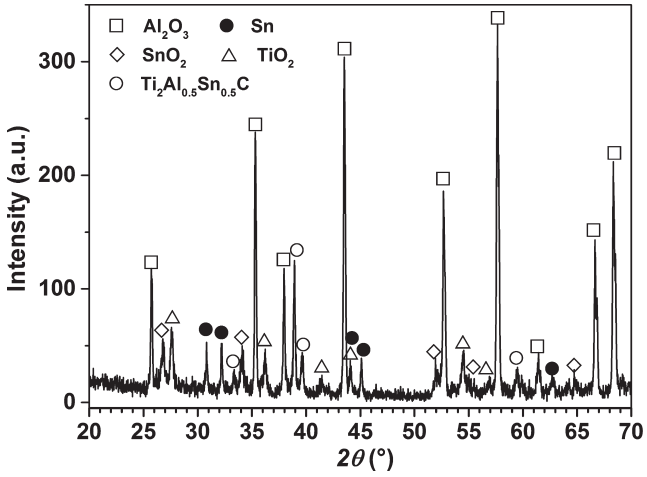

FIGURE 4 X-Ray diffraction pattern of Al_2O_3 composites containing 20 vol.% $Ti_2Al_{0.5}Sn_{0.5}C$ repair filler after heating at 700°C for 48 h

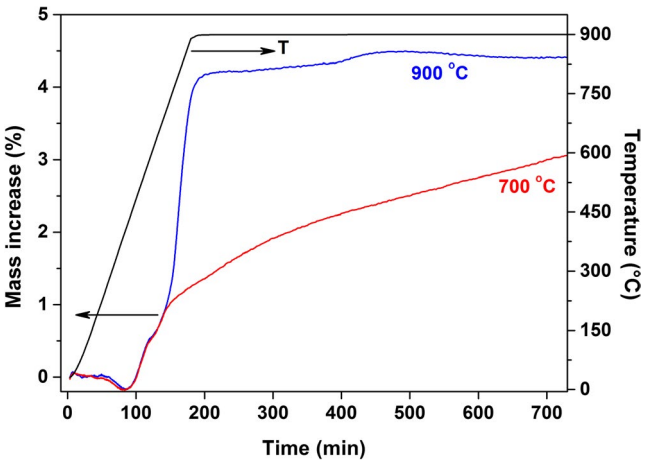

FIGURE 6 Weight gain upon oxidation annealing of the $Ti_2Al_{0.5}Sn_{0.5}C$–Al_2O_3 composite (20 vol.%) in air at 700 and 900°C for 12 h

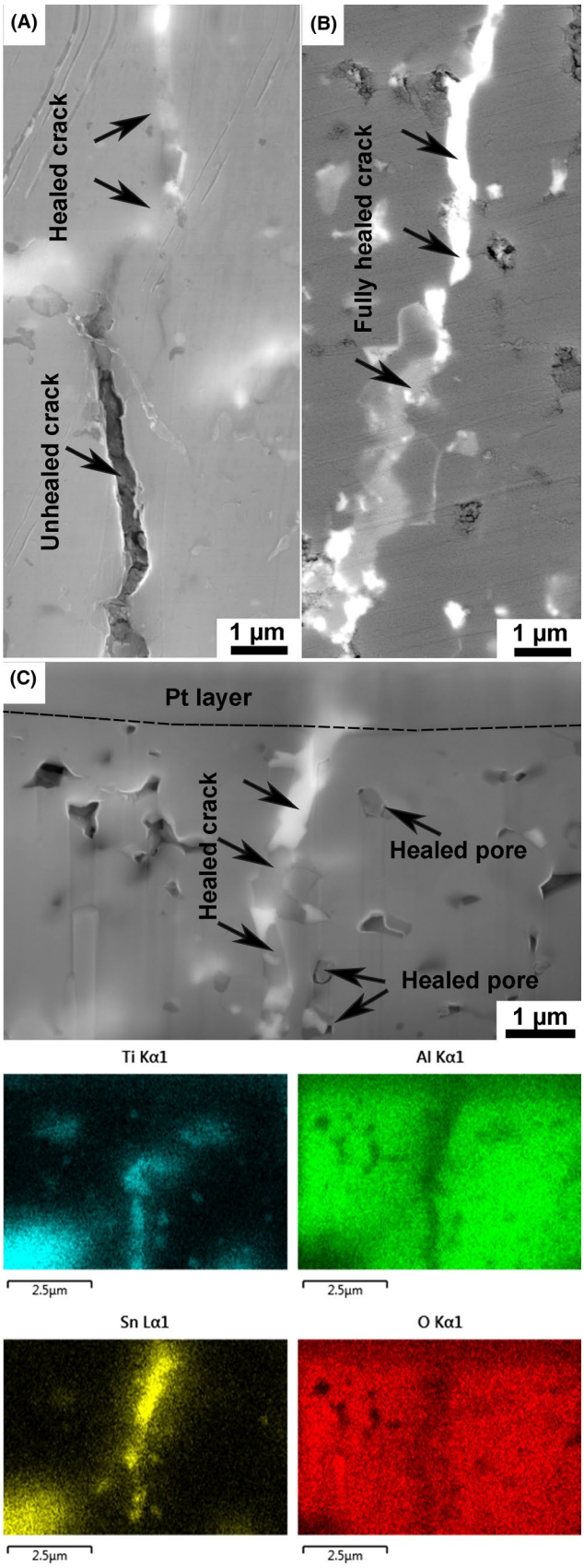

FIGURE 7 Scanning electron microscopy (SEM) micrographs of cracks after annealing at 700°C for 48 h (A) 10 vol.% $Ti_2Al_{0.5}Sn_{0.5}C–Al_2O_3$ composites, (B) 20 vol.% $Ti_2Al_{0.5}Sn_{0.5}C–Al_2O_3$ composites, (C) a cross section of the healed crack in the 20 vol.% $Ti_2Al_{0.5}Sn_{0.5}C–Al_2O_3$ composites prepared by focus ion beam and corresponding SEM-energy dispersive X-ray spectroscopy elemental mapping analysis

Figure 8A is a representative bright field (BF) TEM image showing the Al_2O_3 matrix and the healed area. As indicated in Figure 8A by the white dashed line, an interface clearly separates the Al_2O_3 matrix form the healed zone. Selected area electron diffraction (SAED) confirms the presence of single-crystalline orthorhombic α-Al_2O_3 (see Figure 8B). The healed area, as well as the interface between the α-Al_2O_3 matrix and the healed zone, are examined in more details by high-resolution TEM (HR-TEM). The α-Al_2O_3 matrix exhibits a typical fringe periodicity of 0.21 nm, which fits well with the theoretical lattice spacing of α-Al_2O_3 (113) planes (orthorhombic crystal structure, ICSD #10425). The healed area consists of nanocrystallites (which is evident from Bragg-contrasts in Figure 8A) with a random orientation (see HR-TEM images in Figure 8C,D). The observed spacing of 0.26 nm can be assigned to (104) lattice planes of orthorhombic α-Al_2O_3 (ICSD #10425), while the spacing values of 0.17 and 0.18 nm can be assigned to (211) lattice planes of tetragonal TiO_2 (ICSD #9161) and (211) lattice planes of tetragonal SnO_2 (ICSD #9163), respectively. However, since the lattice spacing values of 0.17 and 0.18 nm are very close to each other, a clear differentiation and their assignment to specific lattice planes is problematic. A misinterpretation of the lattice planes can affect conclusions about the phases, which in this particular case also have an identical (tetragonal) crystal structure with similar lattice parameters. However, in relation and agreement with XRD and SEM-EDXS mapping results, we conclude that both phase, tetragonal TiO_2 and SnO_2, are present (and co-existing with α-Al_2O_3) in the healed zone. Furthermore, amorphous regions are detected at the interface between α-Al_2O_3 and the healed zone, as can be seen in Figure 8C. Also in the interior of the healed zone, an amorphous phase is observed between the nanocrystallites (see Figure 8D). There are two possible reasons for these observations:

1. The annealing temperature of 700°C was relatively low. The temperature may be insufficient for complete crystallization and growth of oxidation products (TiO_2 + SnO_2 + α-Al_2O_3), which is in good agreement with the HR-TEM results from the healed area (Figure 8C,D). According to previous results, a large amount of crystalline TiO_2 (>5 μm) and α-Al_2O_3 (<1 μm) can be expected after annealing at 900°C for 1 hour or above 1000°C.[37,38]

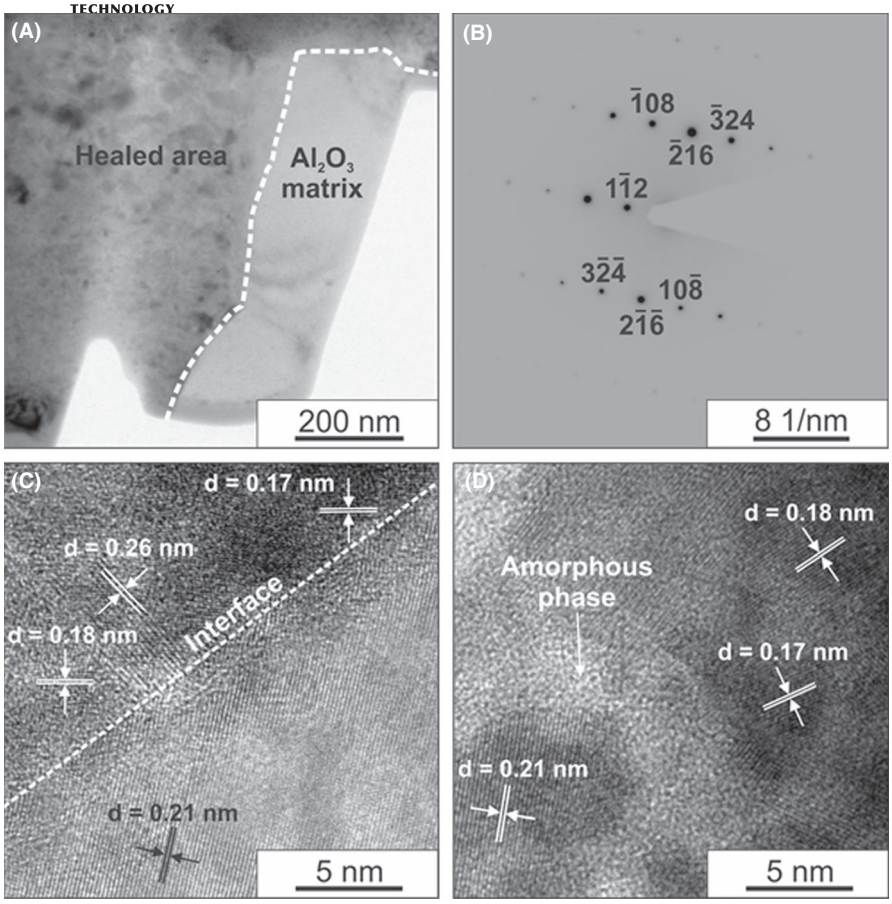

FIGURE 8 Transmission electron microscopy (TEM) analysis of the 20 vol.% $Ti_2Al_{0.5}Sn_{0.5}C$–Al_2O_3 composite after heat treatment at 700°C for 48 h (A) bright field-TEM image of the Al_2O_3 matrix, separated by an interface from the healed area; (B) selected area electron diffraction pattern (valid for the [8 10 1] zone axis) of the orthorhombic α-Al_2O_3 (ICSD #10425); (C) and (D) are high-resolution TEM images, confirming the presence of a single-crystalline α-Al_2O_3 phase, which is separated by an interface from the healed zone, composed of α-Al_2O_3, TiO_2, and SnO_2 nanocrystals

2. Ga^+-ion beam-induced damage during FIB preparation and possible electron beam (e-beam)-induced damage during the TEM analysis may also cause an amorphization of the specimen. Ion-beam-induced damage is often observed during the thinning procedure of the outer regions of TEM samples.[39]

3.3 | Strength recovery

Figure 9 shows the variation of the bending strength prior and after healing treatment at 700°C for 48 and 96 hours. Indentation caused the virgin strength to decrease for more than 50%. After annealing in air, the recovery of strength up to the level of the virgin material (and even slightly higher due to the healing of small surface cracks and pores) can be observed for the composites loaded with 10 and 20 vol.% repair fillers. Since the mean coefficients of thermal expansion of the crack-filling oxide reaction products (TiO_2 [rutile]: 8.4×10^{-6}/K)[40] and SnO_2: 3.9×10^{-6}/K)[41] are smaller than the one of the α-Al_2O_3 matrix material (8.4×10^{-6}/K),[38] compressive stresses are likely to be generated at the crack-matrix interface upon cooling, which tend to increase the crack growth resistance.[32] In addition to healing of the artificial indent cracks, closure of the residual porosity in the composite (2%-7%) might also contribute to the strength recovery.

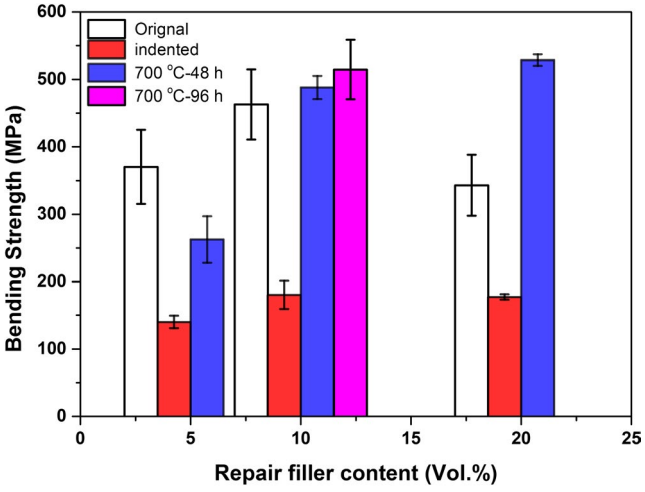

FIGURE 9 Virgin strength, indented strength and recovered strength of the $Ti_2Al_{0.5}Sn_{0.5}C$–Al_2O_3 composites with varied volume fraction of $Ti_2Al_{0.5}Sn_{0.5}C$ repair filler

4 | CONCLUSION

The oxidation-induced crack healing of a Al_2O_3 composite loaded with the $Ti_2Al_{0.5}Sn_{0.5}C$ MAX phase repair filler was examined at 700°C. The formation of nano-sized TiO_2

(rutile) + SnO_2 + α-Al_2O_3, as well as a minor fraction of metallic Sn as the crack-filling material, is observed. Restoration of the solid contact between the crack surfaces triggers complete recovery of the compromised strength at repair filler fractions exceeding 10 vol.%.

ACKNOWLEDGMENTS

The financial support by the German Research Foundation (DFG, GR961/33-2 project) and DFG through the Cluster of Excellence EXC315 "Engineering of Advanced Materials" (EAM) is gratefully acknowledged.

ORCID

Guoping Bei https://orcid.org/0000-0002-9315-6834

REFERENCES

1. Greil P. Generic principles of crack-healing ceramics. J Adv Ceram. 2012;1:249–67.
2. Van der Zwaag S. Self healing materials an alternative approach to 20 centuries of materials science. Dordrecht, the Netherlands: Springer; 2007.
3. Hager MD, Greil P, Leyens C, van der Zwaag S, Schubert US. Self-healing materials. Adv Mater. 2010;22:5424–30.
4. Roberts J, Wrona BJ. Crack healing in UO_2. J Am Ceram Soc. 1973;56:297–9.
5. Bandyopadhyay G, Roberts J. Crack healing and strength recovery in UO_2. J Am Ceram Soc. 1976;59:415–9.
6. Lange FF, Radford KD. Healing of surface cracks in polycrystalline Al_2O_3. J Am Ceram Soc. 1970;53:420–1.
7. Gupta TK. Crack healing and strengthening of thermally shocked alumina. J Am Ceram Soc. 1976;59:259–62.
8. Lange FF, Gupta TK. Crack healing by heat treatment. J Am Ceram Soc. 1970;53:54–5.
9. Gupta TK. Crack healing in thermally shocked MgO. J Am Ceram Soc. 1975;58:143–43.
10. Lange FF. Healing of surface cracks in SiC by oxidation. J Am Ceram Soc. 1970;53:290.
11. Korouš J, Chu MC, Nakatani M, Ando K. Crack healing behavior of silicon carbide ceramics. J Am Ceram Soc. 2000;83:2788–92.
12. Ando K, Takahashi K, Nakayama S, Saito S. Crack-healing behavior of Si_3N_4/SiC ceramics under cyclic stress and resultant fatigue strength at the healing temperature. J Am Ceram Soc. 2002;85:2268–72.
13. Takahashi K, Kim BS, Chu MC, Sato S, Ando K. Crack-healing behavior and static fatigue strength of Si_3N_4/SiC ceramics held under stress at temperature (800, 900, 1000°C). J Eur Ceram Soc. 2003;23:1971–8.
14. Houjou K, Ando K, Liu SP, Sato S. Crack-healing and oxidation behavior of silicon nitride ceramics. J Eur Ceram Soc. 2004;24:2329–38.
15. Ando K, Kim BS, Chu MC, Saito S, Takahashi K. Crack-healing and mechanical behaviour of Al_2O_3/SiC composites at elevated temperature. Fatigue Fract Eng Mater Struct. 2004;27:533–41.
16. Lee SK, Takahashi K, Yokouchi M, Suenaga H, Ando K. High-temperature fatigue strength of crack-healed Al_2O_3 toughened by SiC whiskers. J Am Ceram Soc. 2004;87:1259–64.
17. Nakao W, Ono M, Lee SK, Takahashi K, Ando K. Critical crack-healing condition for SiC whisker reinforced alumina under stress. J Eur Ceram Soc. 2005;25:3649–55.
18. Takahashi K, Uchiide K, Kimura Y, Nakao W, Ando K, Yokouchi M. Threshold stress for crack healing of mullite reinforced by SiC whiskers and SiC particles and resultant fatigue strength at the healing temperature. J Am Ceram Soc. 2007;90:2159–64.
19. Chlup Z, Flasar P, Kotoji A, Dlouhy I. Fracture behaviour of Al_2O_3/SiC nanocomposite ceramics after crack healing treatment. J Eur Ceram Soc. 2008;28:1073–7.
20. Osada T, Nakao W, Takahashi K, Ando K. Kinetics of self-crack-healing of alumina/Silicon carbide composite including oxygen partial pressure effect. J Am Ceram Soc. 2009;92:864–9.
21. Wataru N, Shihomi A. Enhancement of the self-healing ability in oxidation induced self-healing ceramic by modifying the healing agent. Smart Mater Struct. 2012;21:025002.
22. Osada T, Kamoda K, Mitome M, Hara T, Abe T, Tamagawa Y, et al. A novel design approach for self-crack-healing structural ceramics with 3D networks of healing activator. Sci Rep. 2017;7:17853.
23. Barsoum MW. The $M_{N+1}AX_N$ phases: a new class of solids thermodynamically stable nanolaminates. Prog Solid State Chem. 2000;28:201–81.
24. Song GM, Pei YT, Sloof WG, Li SB, De Hosson J, van der Zwaag S. Oxidation-induced crack healing in Ti_3AlC_2 ceramics. Scripta Mater. 2008;58:13–6.
25. Yang HJ, Pei YT, Rao JC, De Hosson J, Li SB, Song GM. High temperature healing of Ti_2AlC: on the origin of inhomogeneous oxide scale. Scripta Mater. 2011;65:135–8.
26. Li S, Song G, Kwakernaak K, van der Zwaag S, Sloof WG. Multiple crack healing of a Ti_2AlC ceramic. J Eur Ceram Soc. 2012;32:1813–20.
27. Yang HJ, Pei YT, Rao JC, De Hosson J. Self-healing performance of Ti_2AlC ceramic. J Mater Chem. 2012;22:8304–13.
28. Li S, Xiao L, Song G, Wu X, Sloof WG, Van Der Zwaag S. Oxidation and crack healing behavior of a fine-grained Cr_2AlC ceramic. J Am Ceram Soc. 2013;96:892–9.
29. Li S, Bei G, Chen X, Zhang L, Zhou Y, Mačković M, et al. Crack healing induced electrical and mechanical properties recovery in a Ti_2SnC ceramic. J Eur Ceram Soc. 2016;36:25–32.
30. Li S, Zhang L, Yu W, Zhou Y. Precipitation induced crack healing in a Ti_2SnC ceramic in vacuum. Ceram Int. 2017;43:6963–6.
31. Pedimonte BJ, Bei G, Pourjafar D, Fey T, Greil P. Oxidative crack healing in Al_2O_3 composites loaded with Ti_2AC (A = Al, Sn) repair fillers. J Ceram Sci Technol. 2014;5:63–8.
32. Bei GP, Pedimonte BJ, Pezoldt M, Ast J, Fey T, Goeken M, et al. Crack healing in $Ti_2Al_{0.5}Sn_{0.5}C$–Al_2O_3 composites. J Am Ceram Soc. 2015;98:1604–10.
33. Boatemaa L, Bosch M, Farle A, Bei GP, Van der Zwaag S, Sloof W. Autonomous high-temperature healing of surface cracks in Al_2O_3 containing Ti_2AlC particles. J Am Ceram Soc. 2018;101:5684–93.
34. Bale CW, Chartrand P, Degterov SA, Eriksson G, Hack K, Ben Mahfoud R, et al. FactSage thermochemical software and databases. Calphad. 2002;26:189–228.
35. Ohji T, Jeong YK, Choa YH, Niihara K. Strengthening and toughening mechanisms of ceramic nanocomposites. J Am Ceram Soc. 1998;81:1453–60.
36. Bei G, Pedimonte BJ, Fey T, Greil P. Oxidation behavior of MAX phase $Ti_2Al_{(1-x)}Sn_xC$ solid solution. J Am Ceram Soc. 2013;96:1359–62.

37. Cui B, Jayaseelan DD, Lee WE. Microstructural evolution during high-temperature oxidation of Ti_2AlC ceramics. Acta Mater. 2011;59:4116–25.
38. Kong F, Feng K, Bai Y, Li N. Oxidation behaviour of high purity nonstoichiometric Ti_2AlC powders in flowing air. J Mater Res. 2017;32:2747–54.
39. Cui B, Jayaseelan DD, Lee WE. TEM study of the early stages of Ti_2AlC oxidation at 900°C. Scripta Mater. 2012;67:830–3.
40. Hummer DR, Heaney PJ, Post JE. Thermal expansion of anatase and rutile between 300 and 575 K using synchrotron powder X-ray diffraction. Pow Diff. 2007;22:352–7.
41. Batzill M, Diebold U. The surface and materials science of tin oxide. Prog Surf Sci. 2005;79:47–154.

How to cite this article: Bei G, Mačković M, Spiecker E, Greil P. Low-temperature oxidation-induced crack healing in $Ti_2Al_{0.5}Sn_{0.5}C–Al_2O_3$ composites. *Int J Appl Ceram Technol*. 2019;00:1–8. https://doi.org/10.1111/ijac.13315